

Measurement of adhesion for thermally sprayed materials

C. C. BERNDT* and C. K. LIN

*The Thermal Spray Laboratory, Department of Materials Science and Engineering,
SUNY at Stony Brook, Stony Brook, NY 11794-2275, USA*

Revised version received 21 May 1993

Abstract—Thermally sprayed coatings have a distinctive microstructure which can be described as '*a three-dimensional layered structure of discs which are interlaced to form a material of composite nature*'. The coatings are normally greater than 25 μm in thickness and can thus be described as bulk coatings. The minimum microstructural detail would be a single splat (often described as a lamella), which is about 5 μm in thickness and up to 80 μm in diameter. This paper focuses on methods used to define and measure the adhesion of coatings or deposits formed by thermal spray technology. The properties distinguished include those of strength and toughness. Measurements such as the tensile adhesion (according to ASTM C633) and double cantilever beam (DCB) tests will be addressed to illustrate the relevance (if any) of such methods to present industrial practice. Acoustic emission studies have also assessed a function termed as the 'crack density function', i.e. a product of the number of cracks and crack size. Other measuring methods applied to this technology include micro-hardness and scratch testing. The former technique has demonstrated that the material properties of coatings are anisotropic, and the latter method is being considered within the biomedical industry to assess the adhesion of hydroxyapatite to orthopedic prostheses. These techniques, among others, may be used for both fundamental understanding of coating performance (i.e. life prediction and cracking mechanisms) and as tests for quality control.

Keywords: Acoustic emission; adhesion; adhesion measurement; coating failure; degradation; double cantilever beam test; fracture mechanics; indentation; lifetime modeling; scratch test; thermally sprayed coatings.

1. INTRODUCTION

1.1. Formation and structure of thermally sprayed coatings

A variety of thermal spray processes are available to deposit thick coatings for a broad range of applications [1–3]. The processes are essentially similar in that a material is heated up by a gaseous medium and simultaneously accelerated and projected onto the substrate. The family of thermal spray processes includes, among other processes, flame spraying, plasma spraying, vacuum plasma spraying (also called low pressure plasma spraying), high velocity oxygen fuel, arc metallization, and detonation gun spraying. The prime distinctions between these spraying processes are the temperature of the process and the velocity of the thermal source used in the process. These process variables control the nature of the materials that can be sprayed. The techniques also differ with regard to their process economics; that is, factors such as the cost of the equipment, the cost of

*To whom correspondence should be addressed.

the feedstock materials and other consumables such as gases, grit blast media, etc. that may limit the viability of a particular process.

Thermal spray technology is not limited to coating substrates but now also encompasses the manufacture of net shapes [4], which can be considered as very thick coatings [up to, say, 1" (25 mm) in thickness] stripped from the substrate (or 'forming tool') and then used directly as an engineered material [5]. The availability of thermal spray processes enables the production of materials of varying composition and structure—the so-called 'functionally gradient materials'.

Several conferences have been devoted to thermal spray and such proceedings [6–8] cover many of the processing variables associated with this technology. In addition, a quarterly journal called the *Journal of Thermal Spray Technology* is now available that covers the complete engineering and scientific arenas of this technology.

Thermally sprayed coatings consist of a layered structure that is highly anisotropic such that individual splats are oriented parallel to the substrate surface [9]. A microstructural cross-section of a thermally sprayed material is illustrated in Fig. 1, where unmelted particles are embedded within the layered structure and also pores exist either totally inside or between each layer [10]. After formation of the coating, the first property criterion for this coating system is 'How well is the coating adhered to the substrate' and it therefore follows 'How can we evaluate this adhesion strength, especially for coatings which are in service?' The intent of this paper is to describe and then discuss methods of

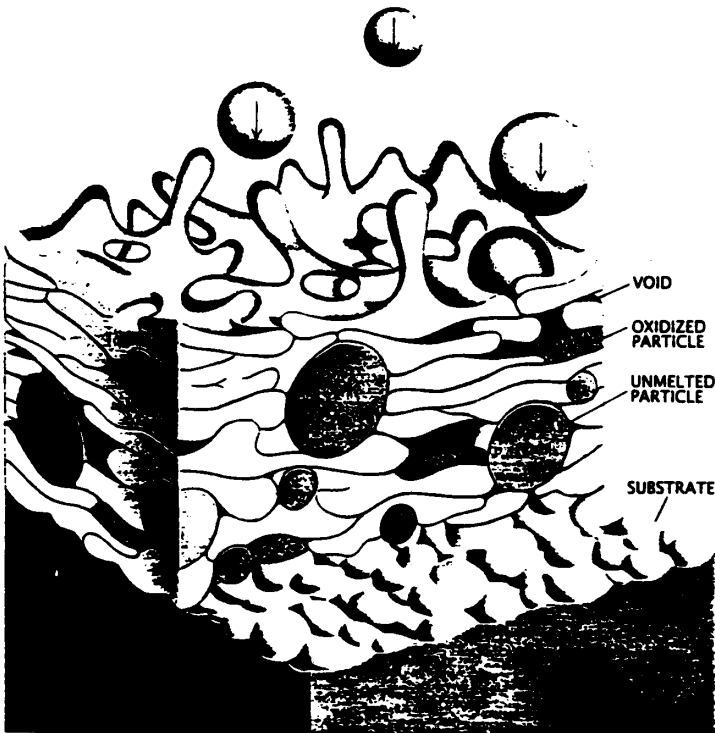


Fig. 1. Microstructure of thermally sprayed coatings [10].

measuring the 'adhesion strength' of thermally sprayed coatings. A strong intent is to always relate such measurements to the ultimate application(s) of the coatings.

1.2. Rationale for measuring adhesion

According to Mittal [11], adhesion can be expressed in various ways. For example, 'basic adhesion' signifies the interfacial bond strength and is the summation of all intermolecular or interatomic interactions. The result of an adhesion test is called 'practical adhesion' and is a function of basic adhesion and many factors—all of which represent the work required to detach a film or coating from a substrate. Many theories or mechanisms for adhesion have been proposed [12, 13]; however, none is fulfilled by all situations and there is no adhesion test available which satisfies all requirements. Therefore the best test method often becomes the one that simulates practical stress conditions.

The term 'adhesion' requires special definition for the purposes of thermal spray coatings. For example, the American Society for Testing and Materials (ASTM) [14] states adhesion as '*the state in which two surfaces may consist of valence forces or interlocking forces or both*'. The theories of adhesion between two materials, in general terms, include mechanisms based on diffusion, mechanical interlocking, electrostatic attraction, physical adsorption, chemical bonding, and weak boundary layers [15]. However, the above global definition cannot be universally applied to thermal spray materials since these coatings can be considered as 'composites' at the microstructural level. Thus, bonding mechanisms for forming an integral coating or net shape will also be complex and may involve adhesion processes which are exclusive of those established for classical joining technology. The basic bonding mechanisms that have been defined for thermal spray coatings can be categorized into three major groups [16] (Table 1).

The specific thermal spraying process will influence the microstructure of the coating and, therefore, it can be inferred that the adhesion strength of the deposit will vary. For example, the high velocity oxygen fuel (HVOF) technique produces a very dense microstructure with porosity typically less than 2% compared to the less than 5% porosity, at best, for a flame sprayed or an atmospheric plasma sprayed material. Thus, factors affected by the spray parameters, including the size and distribution of porosity, oxide content, residual stresses, and macro- or micro-cracks, have an important influence on the performance and eventual failure of the coating system.

Table 1.
The basic bonding mechanisms of thermally sprayed coatings

Mechanical interlocking (anchoring)
Metallic bonds (metal-metal bonds)
dispersion forces
chemisorption and epitaxy
diffusion
Chemical bonds
intermetallic compounds

The service failure mode(s) can be described as interfacial, cohesive, or of mixed **interfacial/cohesive** failures.* This service failure mode must also be reflected by any testing method which seeks to perform a meaningful quality control test of coatings. It is thus preferable that any laboratory test induces the observed service failures, otherwise they will be of limited application to engineering design. Useful measurements on adhesion strength and interpretation of the test results to predict the service life of coatings or net shapes are the most challenging problem for thermal spray scientists.

1.3. Application of fracture mechanics to adhesion measurement

The adhesion of thermally sprayed coatings is not only an interfacial problem of the individual lamella within a coating, but also concerns examination of the integrity of the interface between the substrate and coating, residual stresses, crack population, and pore size and distribution. Fracture mechanics [17, 18] considers the energy required to initiate or propagate cracks and evaluates the adhesion of the coating system in terms of 'fracture toughness, [19–21]. Four-point bending methods, single-edge notched specimens, double cantilever beam tests, indentation techniques, and other measurements have been employed to assess the adhesion of coating systems [22–24].

The purpose of all these methods is fundamentally the same when they are expressed from the viewpoint of fracture mechanics. The experimental proposition is to establish the equilibrium condition where the elastic energy provided by an external force (as defined by the geometry of the specimen and the applied load) is balanced by the propagation of a stable crack. One form of this energy balance criterion derives the strain-energy release rate, G (in J/m^2), and is defined as:

$$G = \frac{\partial(W - U)}{\partial A} \quad (1)$$

where W is the work done by external forces (in J), U is the elastic energy stored in the system (in J), and A is the crack area (in m^2).

It is convenient to write G as

$$G = \frac{F^2}{2B} \frac{dC}{dL} \quad (2)$$

where F is the force required to extend a crack (in N), L is the crack length (in m), B is the thickness (in m), and C is the compliance (in m/N).

The strain-energy release rate can be related to the fracture toughness by

$$K = \sqrt{\frac{EG}{1 - \nu^2}} \quad (3)$$

where E is the elastic modulus (in MPa) and ν is Poisson's ratio (dimensionless).

*Thermal spray engineers should recognize that the term 'interfacial' is used in preference to 'adhesive' to avoid confusion with an 'adhesive' which is used to join materials (i.e. adhesive will be used as a noun rather than as an adjective).

When G exceeds a critical value, G_c , crack propagation occurs and failure of the coating system results. The evaluation of K assumes that both the elastic modulus and Poisson's ratio of the material are known. The physical representation of the above equations is that the change in compliance of the specimen controls the energy input into the creation of new fracture surfaces. Thus, the corollary of this theory is that the crack path and rate of crack growth can be controlled very precisely by appropriate design of the specimen.

Thus, 'mechanical adhesion' can be evaluated in terms of adhesion strength or fracture toughness. Such measurements of coating–substrate adhesion have been reviewed recently and are listed in Table 2 [25–27]. However, test methods for thermally sprayed coatings are restricted. The techniques to be discussed in this paper include the double cantilever beam test, acoustic emission technology, microhardness assessment, and the scratch test. The tensile adhesion test (TAT) is not covered in detail but will be referenced.

Table 2.
Methods that can be used to determine coating–substrate adhesion

Qualitative	Quantitative
<i>Mechanical methods</i>	
Scotch tape test	Direct pull-off method
Abrasion test	Laser spallation test
Bend and scratch test	Indentation test
	Ultracentrifugal test
	Scratch test
<i>Non-mechanical methods</i>	
X-ray diffraction	Thermal method
	Nucleation test
	Capacitance test

2. ADHESION MEASUREMENTS

2.1. Methods

One difficulty with any mechanical property assessment of coatings is how to attach a loading device to the coating without influencing the property that is being measured. Some investigators [28] have approached this problem by manufacturing a pin or disk that could be removed from a mating component (Fig. 2). The surface of this assembly was thermal sprayed and then the pin or disk, depending on the assembly used, removed. The force at fracture was used to find a parameter termed 'the adhesion strength' of the coating. The corresponding shear test is performed by spraying the outside diameter of a cylinder or the head of a pin (Fig. 3) [29]. One potential difficulty with the above test is that the duplex nature of the specimen assembly may influence the coating quality since the heating and cooling behavior of the deposit will be affected by the interface between the two components. Another feature of both the tensile and the shear tests is that the fracture mode is ambiguous since mixed mode failure often occurs.

Other geometries that do not need an adhesive are illustrated in Figs 4 [30] and 5 [31]. These tests have not been widely implemented outside of their

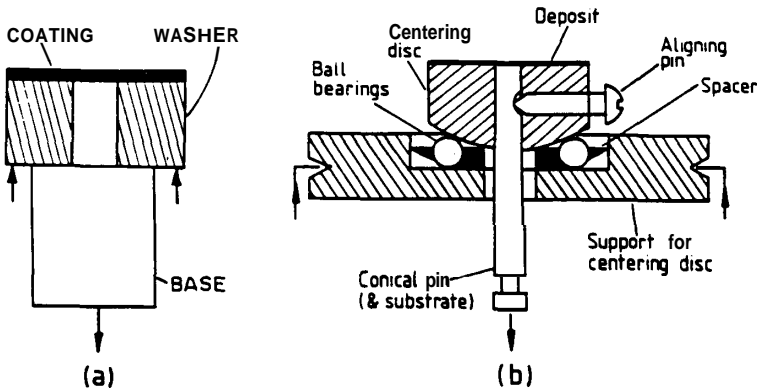


Fig. 2. (a) Specimen for determining adhesion strength; (b) centering device and specimen in cross-section [28].

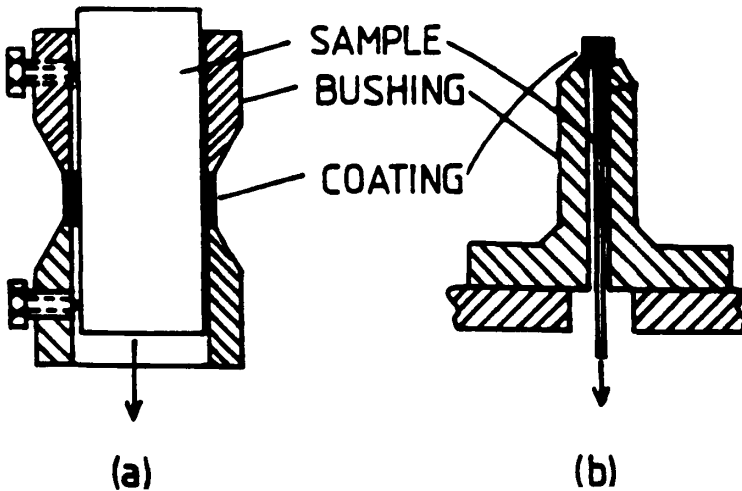


Fig. 3. Shear tests [29].

laboratories of origin. The method of spraying two adjoining conical parts is expected to incorporate a failure which has a large shear component, whereas the other shear test may exhibit either shear failure parallel to the substrate surface or shear failure through the coating thickness.

The adhesion properties of coatings were investigated on the microscopic level [32] by shearing individual particles from the substrate surface (Fig. 6). This study considered that adhesion to the substrate arose from interactions across the particle-substrate interface and a 'strength of growth rate constant' (K') was defined as

$$K' = -\frac{1}{t} \ln \left(1 - \frac{N(t)}{N_0} \right) \quad (4)$$

where t is the time, $N(t)$ is the number of atoms that react during the interaction

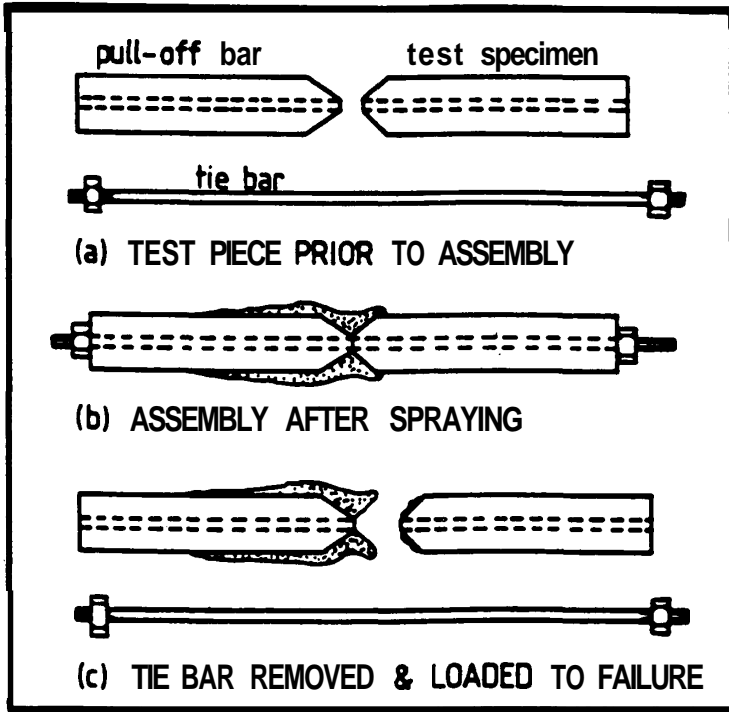


Fig. 4. Adhesion test piece [30].

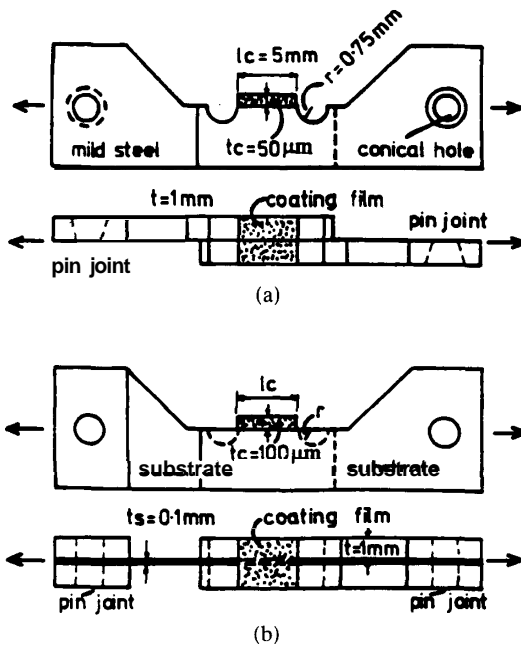


Fig. 5. (a) Shear stress deformation; (b) critical shear stress of adhesion [31].

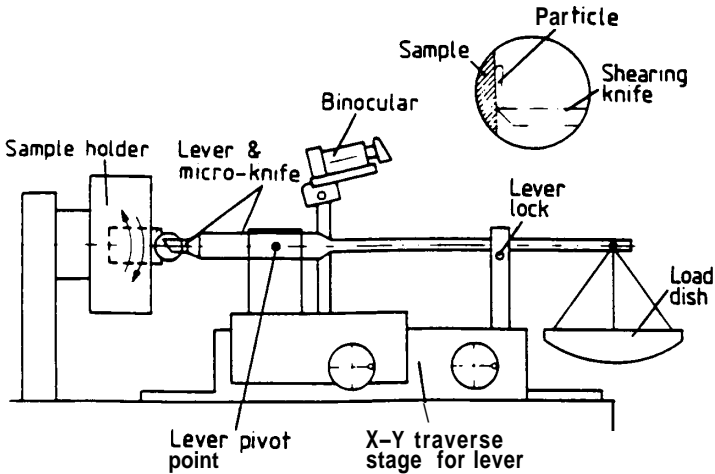


Fig. 6. An instrument for measuring the adhesion strength of the particles [32].

time, and N_0 is the number of atoms in the particle and substrate that are in contact.

The upshot of this analysis was that the strength of the coating at some interaction time of ' t ' was compared with the maximum strength of the coating at the end of the thermal spray process. It was established that the extent of the particle/interface reaction increased with both increasing particle pressure and temperature, and this agreed with the experimental observations that coating adhesion also increased under these conditions. Further theoretical work [33] has treated adhesion as a stochastic process which depends on the formation characteristics of the first monolayer of material. The coating buildup is treated as a statistical process involving input data from the thermal spray processing parameters such as the relative motion between the torch and substrate (i.e. the spray pattern), the velocity and temperature distribution of the thermal source, and the particle size.

2.2. Application of adhesion measurements

The reason for performing adhesion measurements can be brought into focus by examining how such experiments are used to ascertain the utility of coatings. For example, bond strength measurements allow optimization of different grit blast media and the angle of grit blasting, as well as establishing the best coating thickness for aluminum coatings (Fig. 7) [34]. Other workers [35] have optimized ceramic compositions and plasma spraying parameters with respect to strength. Thus, the historical basis for these measurements is significant. In recent years, with the adoption of design of experiment methods [36], bond strength measurements along with other physical measurements (roughness, porosity, etc.) have been used to establish specifications to select coatings.

The strength of the specimen may not be the same as the strength of the engineered coating. It can also be difficult to establish how process-induced residual stresses influence the strength measurements. The adhesion measurement is now taken as a control parameter that can be used as a guide to optimize

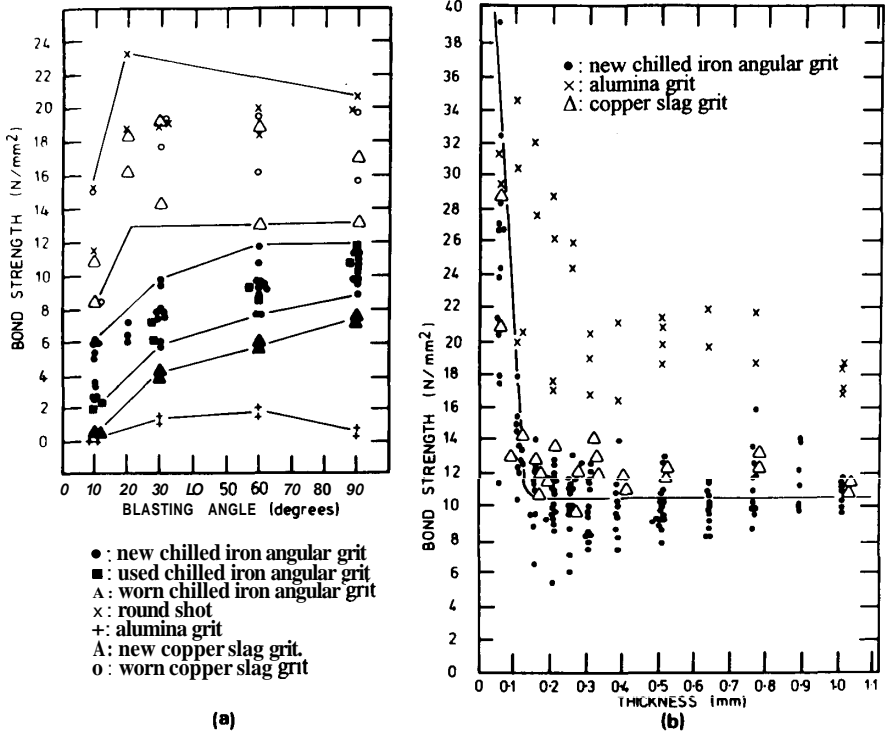


Fig. 7. Variation of the bond strength of aluminum coatings with (a) the blasting angle and (b) the coating thickness [34].

the many process parameters that are involved during thermal spraying. Often the tensile adhesion test is performed as a quality control test and numerous references can be found in thermal spray conference proceedings [6–8].

2.3. Fracture mechanics approach

2.3.1. Overview. The fracture mechanics approach to evaluate crack propagation is based on defining adhesion in terms of a stress intensity factor K or strain-energy release rate G . Methods of measurement include the double cantilever beam (DCB) test; the double torsion test; the bending (three-point or four-point), single-edge notched test; and the compact tension test. Among these, the DCB method allows multiple fracture toughness readings by testing a single specimen and will be discussed in the following section.

The fracture mechanics mode of failure is also a material property that can not only be controlled (to some degree), but must be quantified for engineering design purposes. Thus, a major justification for a fracture mechanics test is that a mode I (tensile) or a mode II (shear) test can be performed and the response of pre-existing flaws ascertained. There is also the possibility of carrying out mixed mode tests that may better replicate a variety of service conditions that the coating may experience throughout its lifetime.

The double torsion test [37, 38] has been applied to thermally sprayed coatings (Fig. 8). The prime advantage of this test is that there is no need to measure the

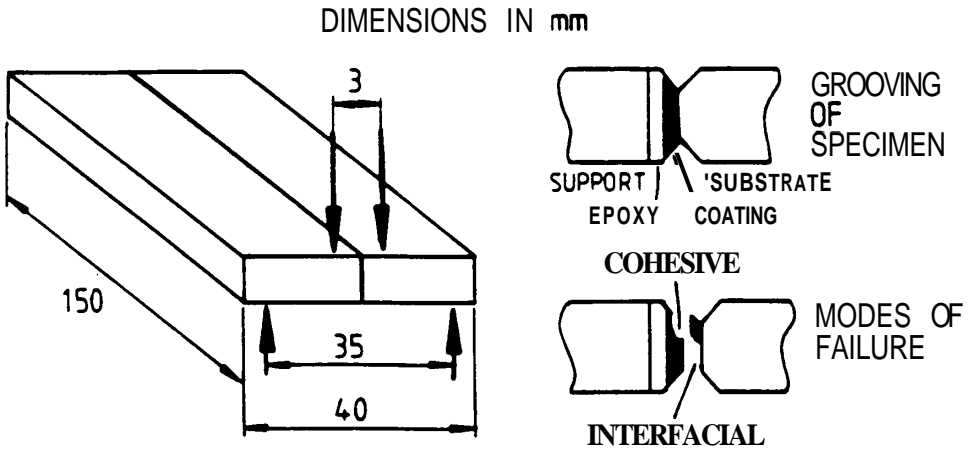


Fig. 8. Double torsion geometry and test configuration.

crack length because cracking occurs at a constant strain-energy release rate or stress intensity factor. Specimen manufacture involves incorporating the coating into an arrangement so that a torque can be applied to the crack front. The shortcomings of the test are that mode I cracking, where the crack front is orthogonal to the crack propagation direction, was never verified despite several attempts. It also appeared that both arms of the double torsion specimen were deflecting at a constant angle along their entire length. Both these conclusions are reflected in the fracture surface morphology as indicated in the inset diagram (on the bottom right) of Fig. 8 where a mixed mode of failure is observed.

The four-point bending test has also been applied to measure the fracture toughness of ceramics joined with metals [39]. The configuration is quite simple and one measurement can be obtained from each test.

2.3.2. Double cantilever beam (DCB) test. A major advantage of the DCB test is that it may have wide applicability to the design engineer; however, this ideal comes at the expense of complex specimen preparation and more sophisticated experimental techniques than the quality control departments of thermal spray shops may be prepared to undertake.

Many configurations of this test are available (Fig. 9) and an example of the technique on a thick film conductor of alumina is shown in Fig. 10 [40]. The applied moment method was used in this case since the crack length, a difficult property to measure for these opaque coatings, was not required. These studies are analogous to those on thermal spray coatings (Fig. 11) [41], where interfacial and cohesive modes of failure were distinguished in terms of fracture toughness. Another DCB geometry arrangement is illustrated in Fig. 12 [42], where a single contoured arm was used.

The general nature of the force vs. displacement requirement of a DCB experiment is shown in Fig. 13. The elastic energy of the specimen arms controls the amount of energy which is transferred to the creation of new crack faces within the locus of fracture. Thus, crack growth, as indicated by the dashed line in Fig. 13, will continue until a stable condition is reached and crack propagation

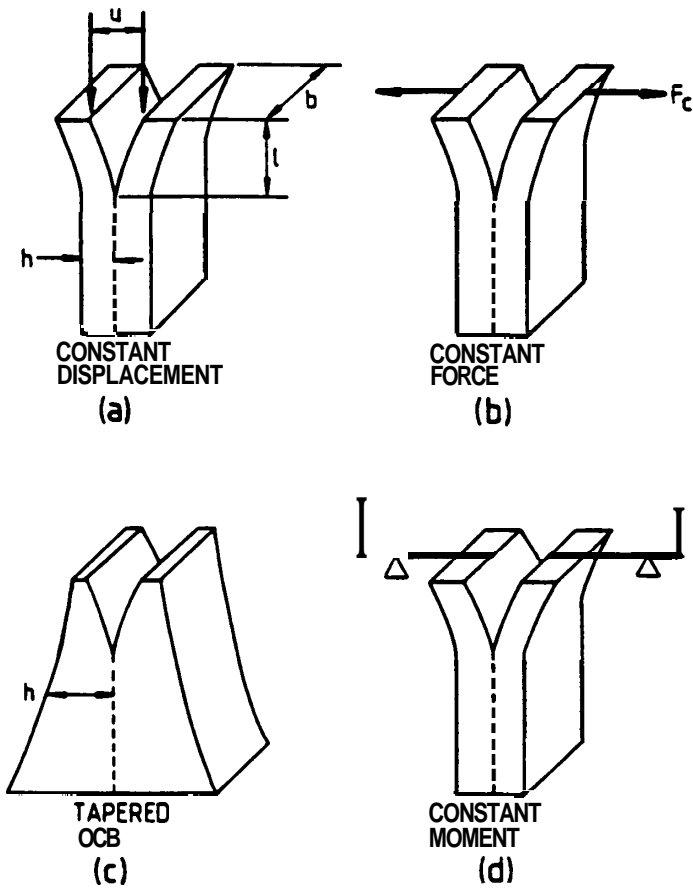


Fig. 9. Double cantilever beam test pieces.

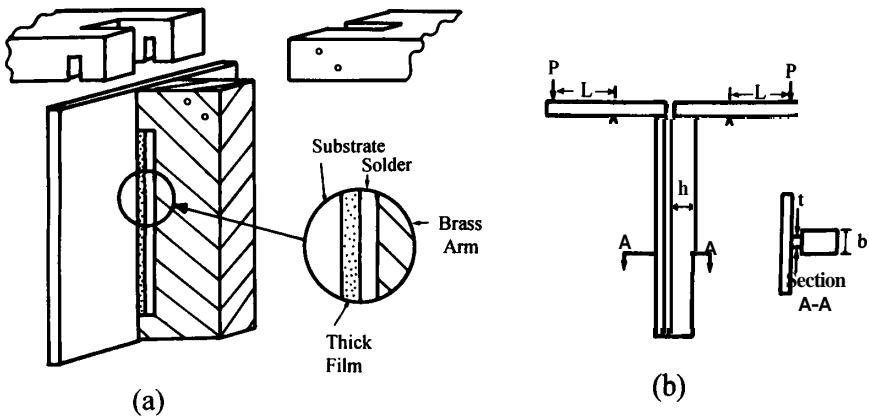


Fig. 10. Applied moment DCB specimen for measuring the adhesion of thick films. (a) Specimen preparation; (b) testing arrangement [40].

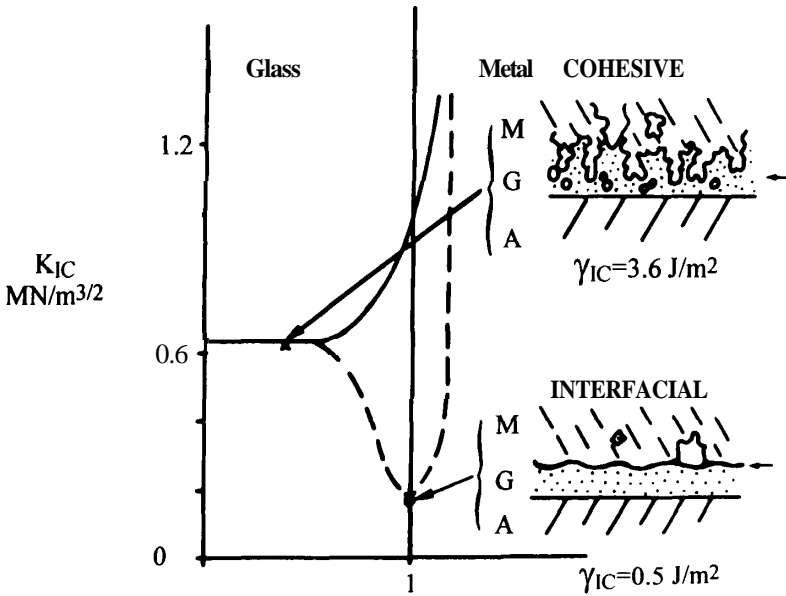


Fig. 11. Model of stress intensity profile through the film and substrate [41]. (In the detailed figure, M is metal, G is glass, and A is alumina.)

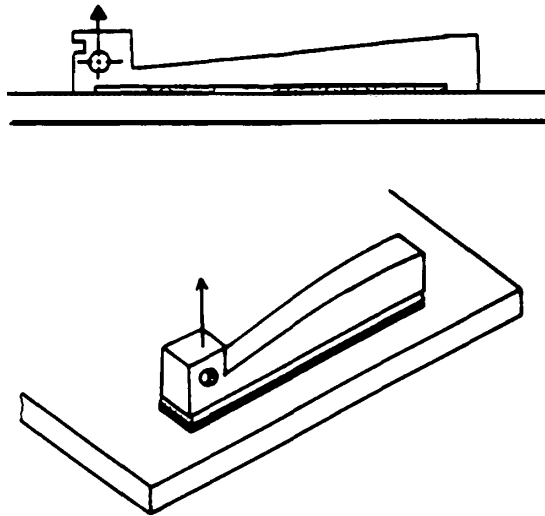


Fig. 12. Specimen with DCB geometry in which one arm is contoured [42].

stops at that point. The new slope of the force–displacement curve (i.e. the compliance) indicates the magnitude of the new crack length, and the area enclosed within the force–displacement curve is related to an energy transfer (from the DCB arms to the crack) during crack growth. Thus, the versatility of the DCB method is that the energy input into the coating can be controlled by altering the elastic modulus and/or geometry of the DCB arms.

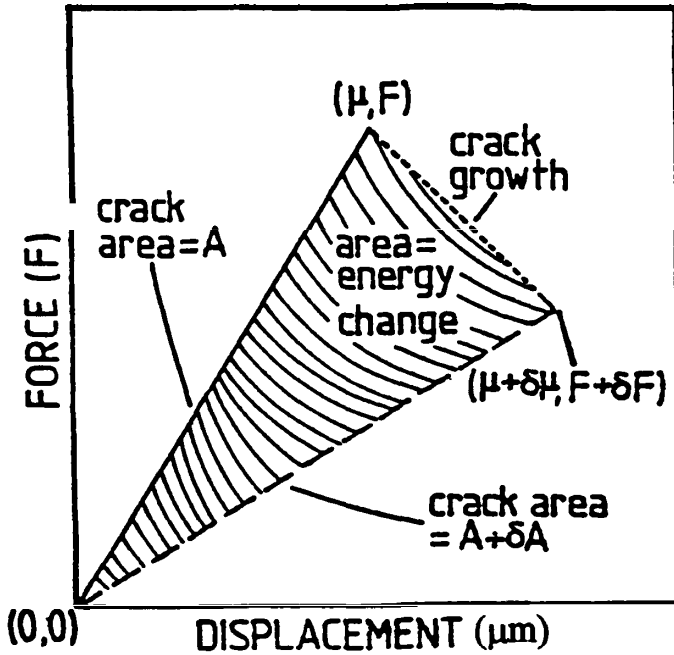


Fig. 13. Energy change when a crack grows.

It is also necessary to verify that the arms of the DCB are indeed bending and that there is no rigid movement of the adherends (Fig. 14a). It was established that true bending of the DCB arms did take place as indicated in Fig. 14c, rather than the ideal situation as depicted in Fig. 14b. The composite DCB geometry which incorporated an adhesive joint does not directly obey the Mostovoy formulation [43] but a modified equation that incorporated displacement at the crack-tip and deformation beyond the crack-tip fitted reasonably well to the theory (Fig. 15).

2.3.3. DCB test for thermally sprayed materials. In the basic DCB test on coatings (Fig. 16), a tension force is applied to the specimen assembly and displacement is measured by an extensometer placed on the arms [22]. When cracking initiates, as noticed by load decreasing with extension increasing, the DCB is unloaded. Several loading/unloading sequences are performed until complete failure of the specimen, at which point the morphology can be examined by optical microscopy and scanning electron microscopy (SEM). Either one of the three failure modes, i.e. interfacial, cohesive, and mixed, can be observed and both inter- and trans-lamellar cracking is exhibited. The locus of fracture can be controlled by grooving the edges of the DCB as shown in the inset (right-hand side) of Fig. 16. Another feature of the DCB method is that the method is not limited by the strength of the adhesive, as is the case for tensile adhesion tests but since it is a fracture mechanics test, it is only necessary for the fracture toughness of the adhesive to be greater than that of the coating. This is a relatively easy condition to satisfy.

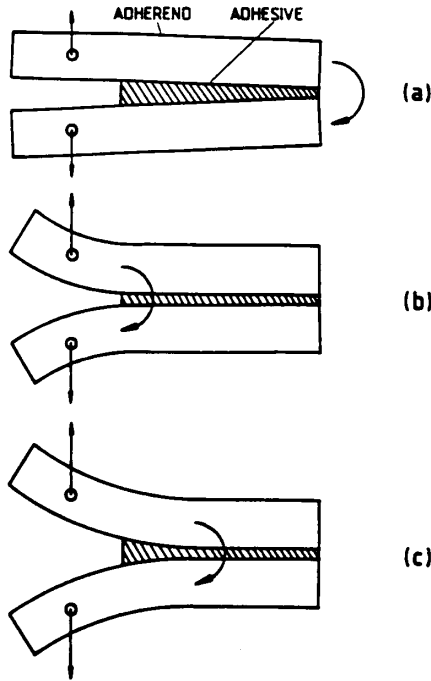


Fig. 14. Bending modes of a DCB specimen. (a) Rigid arms; (b) cantilever beams built in at the crack-tip; (c) rotation of cantilever beams at a point beyond the crack-tip.

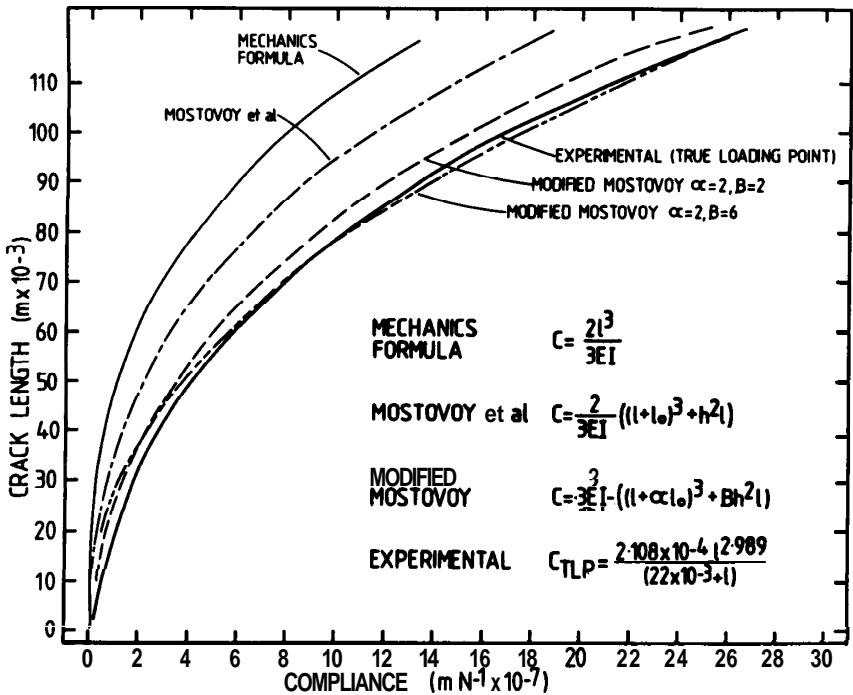


Fig. 15. Experimental compliance–crack length functions compared to various theories.

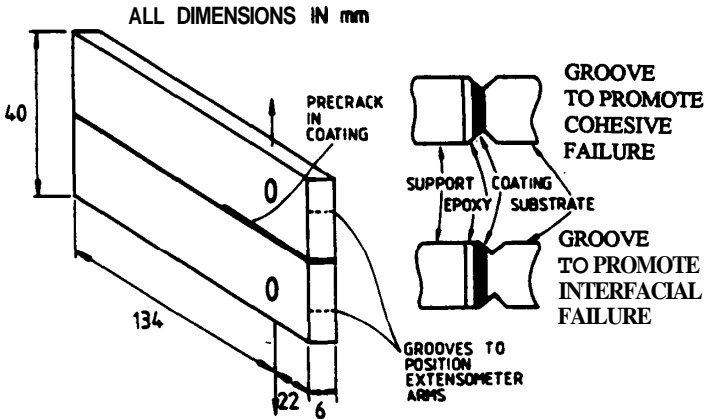


Fig. 16. DCB specimens used for adhesion measurement. The inset shows the grooving procedure to promote either interfacial or cohesive failure.

2.3.4. G_{IC} *determination*. The critical strain-energy release rate, G_{IC} , is determined from equation (2). The compliance values, dC/dL , are determined from the displacement at the loading points (C_{LP}), which differs from the values recorded by the extensometer which is termed the crack opening displacement (C_{COD}). An experimentally determined calibration curve is necessary to calculate dC/dL [22, 44]. Several laboratories have used this technique [45, 46] to generate G_{IC} data. The results are compiled with fracture indentation measurements in Table 3. The mean G_{IC} values for ceramic coatings exhibit a large range but generally they can be considered to lie below $\approx 100 \text{ J/m}^2$, whereas G_{IC} values for metallic coatings are greater than 100 J/m^2 .

Table 3a.
 G_{IC} values (in J/m^2) for thermally sprayed alumina coatings'

Material	Mean	SD	Method	Note	Ref.	Appendix
Al_2O_3	12	2	DCB	IF	22	Metco 101
Al_2O_3	16.1	5.3	DCB	CF	23	Metco 105
Al_2O_3	21	5	DCB	CF	22	Metco 101
Al_2O_3	31.6	9.3	DCB	CF	23	Sealed
Al_2O_3	34	9	DT	CF	22	Metco 101
Al_2O_3	49.8	14.0	DCB	CF	23	PC-WAF
Al_2O_3	52.7	14.5	DCB	CF	23	As sprayed
Al_2O_3	58	16	DCB	Int. BC Fail.	22	Metco 101
Al_2O_3	78	29	DT	IF	22	Metco 101
Al_2O_3	209	—	Ind.	Load: 47 N	23	—
Al_2O_3	189	—	Ind.	Load: 98 N	23	—
Al_2O_3	97.6	—	Ind.	Load: 147 N	23	—
Al_2O_3 -2.5 wt% TiO_2	15.9	5.6	DCB	CF	23	—
Al_2O_3 -2.5 wt% TiO_2	218	—	Ind.	Load: 73.5 N	23	—
Al_2O_3 -2.5 wt% TiO_2	268	—	Ind.	Load: 147 N	23	—
Al_2O_3 -2.5 wt% TiO_2	301	—	Ind.	Load: 98 N	23	—
Al_2O_3 -40% TiO_2	48.7	15.8	DCB	IF	23	—

^a For data given in K, equation (3) is used to convert K into G by assuming $E = 48 \text{ GPa}$; $\nu = 0.25$.

SD: standard deviation; IF= interfacial failure; CF= cohesive failure; Int. BC Fail.: interfacial bond coat failure; Ind.: indentation.

Table 3b. G_{IC} values (in J/m²) for thermally sprayed zirconia coatings"

Material	Mean	SD	Method	Note	Ref.
ZrO ₂ -10 CeO ₂	11.4	3.6	DCB	IF	21
ZrO ₂ -15 CeO ₂	74.1	22.9	DCB	IF	21
ZrO ₂ -15 CeO ₂	125.4	51.1	DCB	CF	21
ZrO ₂ -6 Y ₂ O ₃	49.9	16.7	DCB	IF	21
ZrO ₂ -6 Y ₂ O ₃	95.5	39.4	DCB	CF	21
ZrO ₂ -6 Y ₂ O ₃	148.3	52.3	DCB	Mixed	21
ZrO ₂ -20 Y ₂ O ₃	30.0	10.4	DCB	IF	21
ZrO ₂ -20 Y ₂ O ₃	69.7	31.8	DCB	CF	21
ZrO ₂ -20 Y ₂ O ₃	43.2	19.6	DCB	Mixed	21
ZrO ₂ -8 Y ₂ O ₃	11.1	1.3	Ind.	Load: 50 N	68
ZrO ₂ -8 Y ₂ O ₃	10.4	1.3	Ind.	Load: 100 N	68
ZrO ₂ -8 Y ₂ O ₃	16.0	1.0	Ind.	Load: 50 N	68
ZrO ₂ -8 Y ₂ O ₃	21.2	1.2	Ind.	Load: 100 N	68
ZrO ₂ -8 Y ₂ O ₃	5.7	0.9	Ind.	Load: 50 N	68
ZrO ₂ -8 Y ₂ O ₃	3.8	0.5	Ind.	Load: 100 N	68
ZrO ₂ -8 Y ₂ O ₃	5.3	0.5	Ind.	Load: 50 N	68
ZrO ₂ -8 Y ₂ O ₃	5.8	0.7	Ind.	Load: 100 N	68
YSZ	24.0	6.4	Ind.	Load: 588 N	65

"For data given in K, equation (3) is used to convert K into G by assuming $\nu = 0.25$. Mixed: mixed mode failure.

Table 3c. G_{IC} values (in J/m²) for thermally sprayed coatings of some metals and ceramics^a

Materials	Mean	SD	Method	Note	Ref.
Mild Steel	116	21	DCB	IF	22
Mild Steel	261	71	DCB	CF	22
Ni-Al	319	95	DCB	CF	22
Cr ₂ O ₃	43.0	5.2	Ind.	Load: 9.8-98 N	64
Spinel	47.0	12.7	Ind.	Load: 294 N	65
Ti	6.79	0.34	4-P Bending	With stress	39
Ti	2.98	0.19	4-P Bending	Without stress	39
Ni-20% Al	362	16	DCB	CF	23

"For data given in K, equation (3) is used to convert K into G by assuming $\nu = 0.25$.

2.4. Acoustic emission

2.4.1. Background. Acoustic emission (AE) is a term describing a class of phenomena whereby transient elastic waves are generated by the rapid release of energy from localized sources within a material.' [47]. The energy usually arises from one or more sources [48], which include phase transformation, plastic deformation, corrosion, and crack initiation and growth [49]. An AE event is detected by a piezoelectric transducer when energy is released from the material. The output is amplified and then features of the AE signal such as the ring down count, rise time, and/or pulse height are subjected to analysis. Often a multi-channel system is used to examine different energy levels and the signal may also be digitized or integrated for an energy analysis.

Special interest lies in formulating crack initiation and growth criteria which

are based on the microstructural design of coatings. This is important because microstructural features can be quantitatively determined [50] by image analysis methods and leads to the conclusion that the microstructure of coatings can be 'controlled' by the thermal spray process. **AE** technology has been combined with fracture mechanics measurements [51–53] or thermal tests [54, 55] to characterize coating properties. **AE** technology has been applied to better understand failure mechanisms and to predict lifetimes [56–58]. It has also been applied to quality control and in-service monitoring.

2.4.2. Crack density function. A thermal spray coating has a very rich microstructure, and both macro- and micro-cracking, among other sources, can release energy during coating service. A difficulty is that the **AE** response is overwhelming with regard to acquiring data and this often limits the **AE** method to be a qualitative technique since individual **AE** response-to-coating morphology correlations cannot be made. However, quantitative **AE** analysis may still be possible through a test procedure which is combined with calibration [59, 60]. For example, studies on thermal barrier coatings that were subjected to heat cycling changed from a systematic response to a stochastic response during a certain thermal cycle. This was considered to be indicative of a change in cracking response from micro- to macro-cracking since the change in **AE** response was correlated to the observation of the formation of large cracks (Fig. 17) [61].

The record of **AE** response for coatings will be a combination of all possible noise origins, and a 'crack density function' (CDF) [62] which incorporates both the number of cracks and the size of cracks has been proposed. It is found that macrocracking events tend to occur at low values of the CDF. Figure 18 shows an example of a CDF analysis for two coatings that were prepared to exhibit different behaviors. The essential details are that one sample (indicated by the filled-in parts of the histogram) exhibited a lower frequency of the CDF function and this is indicative of a lower degree of cracking, in terms of both the number of cracks and the size of cracks (since the CDF incorporates these physical characteristics of coatings). At failure and after failure (Figs 18b and 18c), the frequency of these events increased.

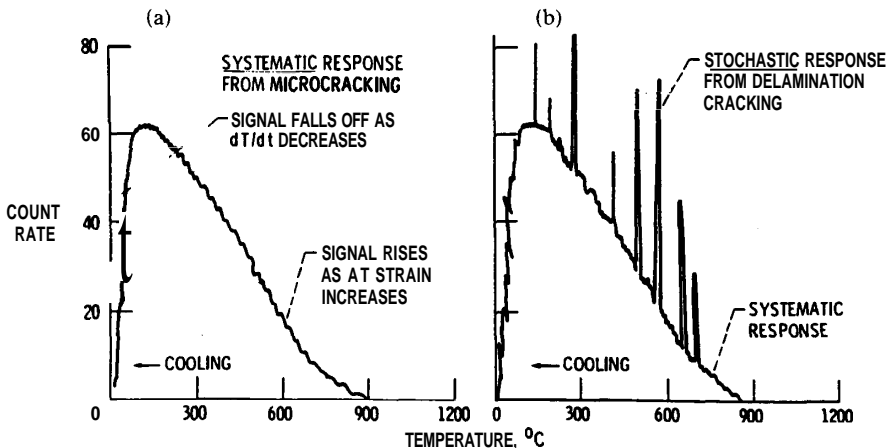


Fig. 17. Schematic diagram of AE effects. (a) Typical cooling cycle; (b) failure during cooling cycle.

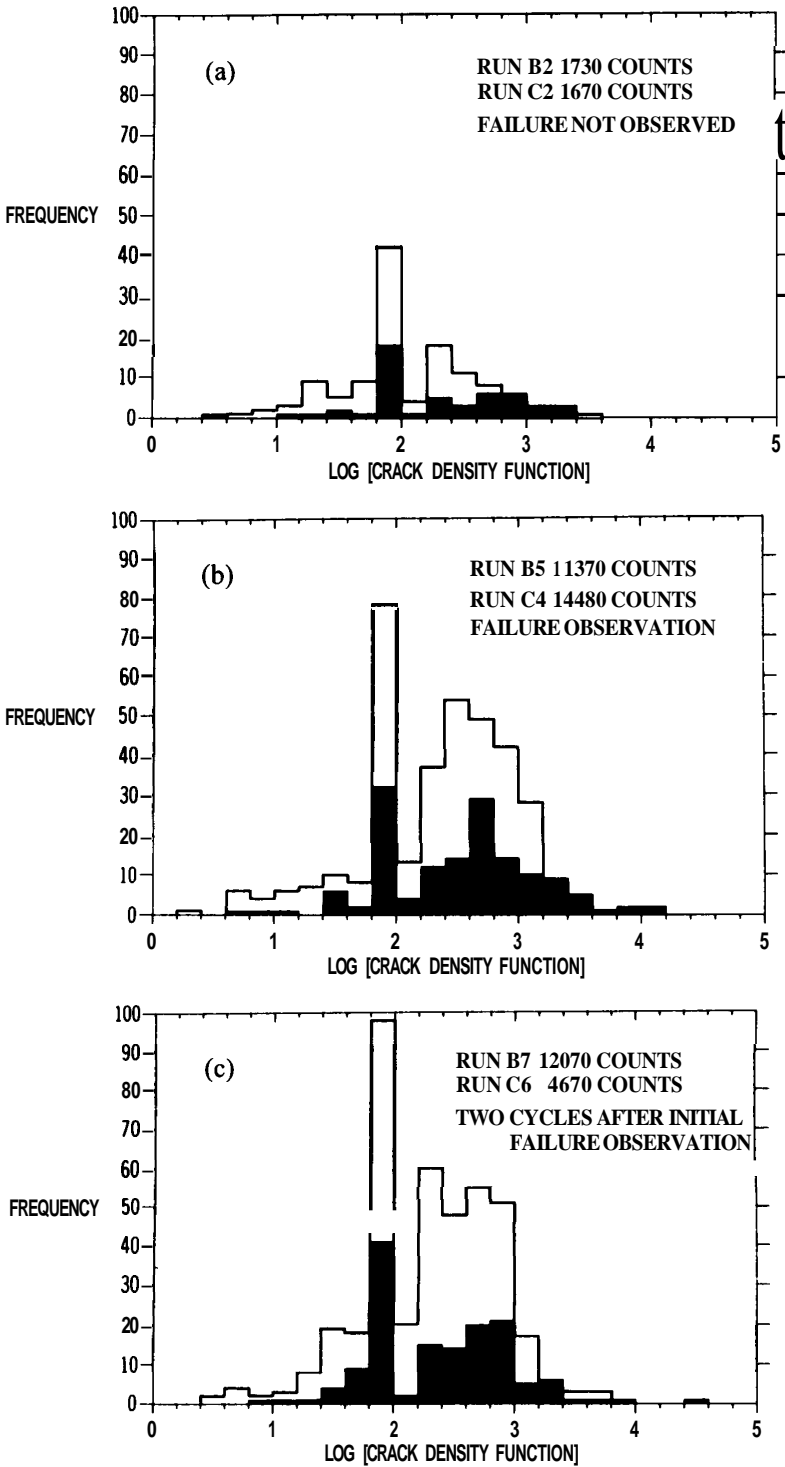


Fig. 18. Crack density function analysis of coatings. (a) First thermal cycle; (b) failure cycle; (c) two cycles after failure.

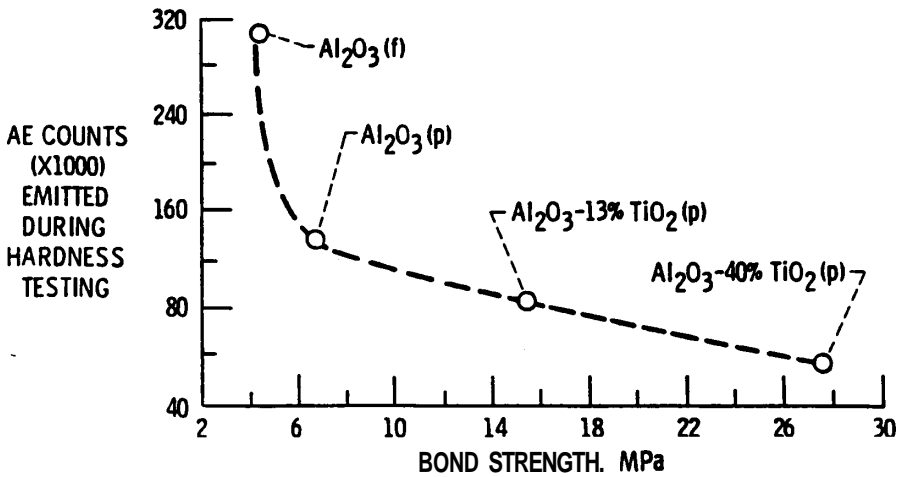


Fig. 19. Bond strength vs. AE emitted during hardness testing.

AE methods have also been used in conjunction with mechanical property measurements. For instance, it has been established that the number of AE counts emitted during a hardness test increases as the density of the material decreases. Figure 19 indicates a number of processes and materials where it is generally understood that flame spraying (indicated by 'f') will produce a less dense deposit than plasma spraying ('p') and also that additions of titania to alumina increase the deposit density. Thus, an intuitive interpretation is that the most dense material exhibits the least cracking behavior and this is reflected in a lower AE response.

Similar correlations have been proposed on the basis of AE measurements performed during tensile adhesion tests (TATs). The AE count accumulated during a TAT is graphed with respect to the so-determined bond strength in Fig. 20. The coatings which incorporate metallic constituents exhibit an activity lower than that of the non-metallic coatings (at equivalent bond strengths). Therefore, a physical interpretation of the mechanical response is that the metallic materials allow more plastic deformation than the ceramic materials. This simple explanation relates well to the general understanding of bulk material behavior, i.e. ceramics are more brittle than metals. However, one caution is that such correlations between bulk material properties and thermally sprayed materials may not be correct since these thick coatings are formed by a rapid solidification process.

The purpose of this discussion is to show that adhesion and cracking mechanisms are symbiotic material properties that can be linked by AE processes. Thus, in a very broad sense, a study and understanding of cracking mechanisms will lead to real improvements in maximizing the adhesion of coatings. For example, consider relating the AE response during a TAT to the cracking and deformation behavior of the specimen assembly. Figure 21 is a schematic diagram which indicates that the strain in the bond coat (the metallic constituent) is always greater than the ceramic strain, although the absolute extension in the ceramic layer is greater than that of the bond coat. The overall view is that cohesive failure occurs by many microcracks throughout the material, whereas interfacial failure has a lower density of cracks. The other implication

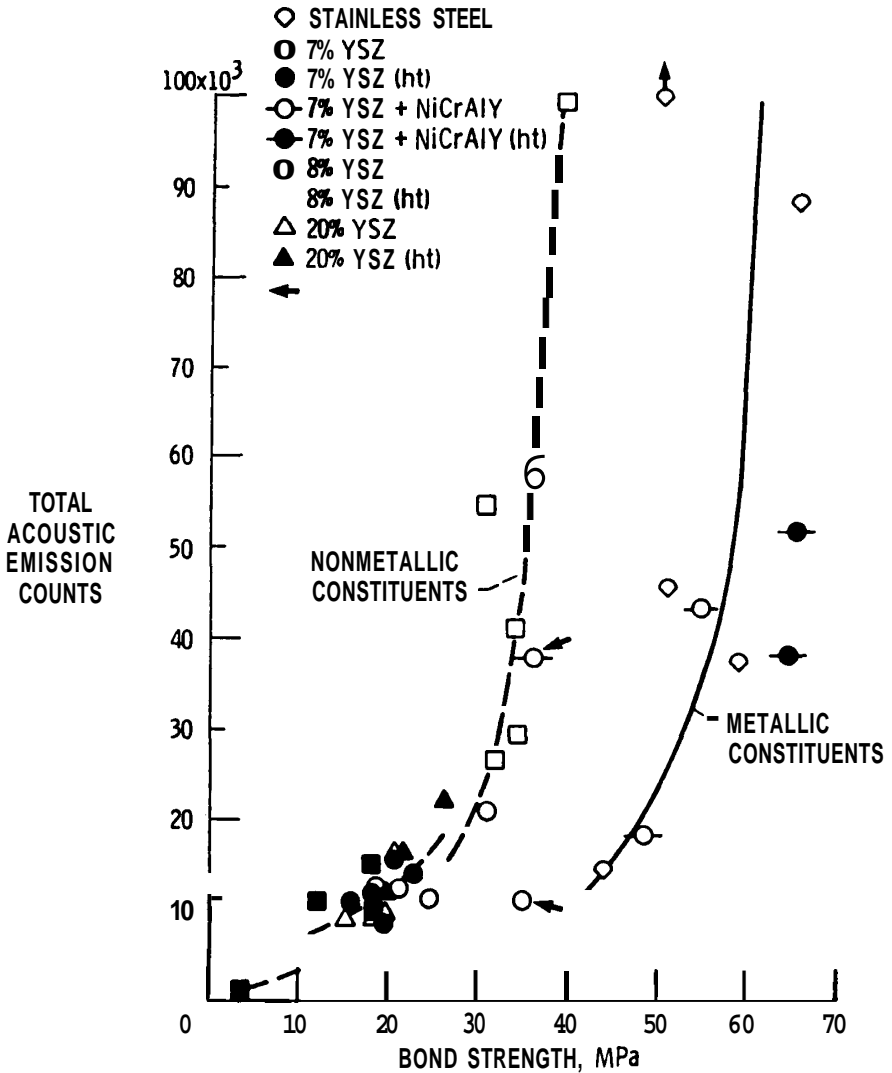


Fig. 20. Bond strength vs. AE emitted during tensile testing.

from Fig. 21 is that cracking during a TAT always begins at the edges of the material and that flaws in this region may dictate the so-determined strength value since they are the weakest link.

2.5. Microhardness assessment

2.5.1. Indentation fracture toughness. Indentation techniques are often used as surface characterization tests. The hardness, implying the resistance of a material to permanent indentation, is measured by a sharp or blunt indenter. Specific crack patterns can be observed [63] in the material at certain loads on the indenter. The indentation method allows the fracture toughness of materials [64–66] and, in particular for thermal spray coatings, the properties of the interface between the

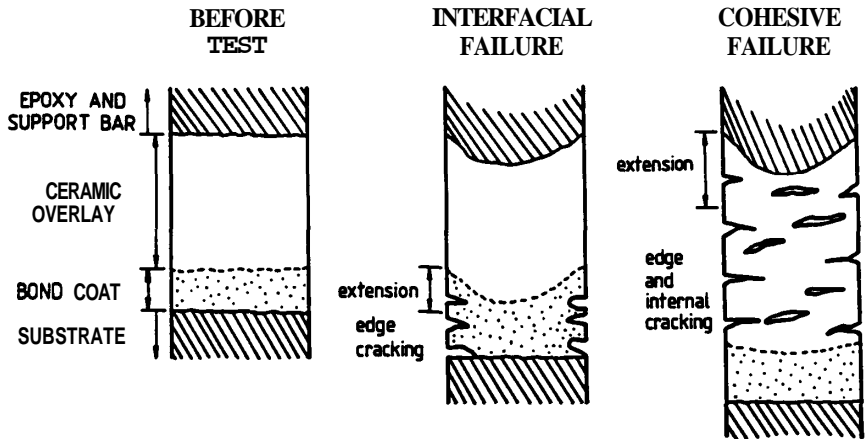


Fig. 21. Schematic diagram to illustrate the coating deformation response during the interfacial and cohesive failure modes.

coating and substrate to be measured. The coating toughness has been measured by the Vickers indentation test [67, 68], where it is necessary to measure the indent diagonals and the crack lengths produced during the test.

The results of several workers have been summarized in Table 3. The indentation fracture toughness measurements tend to be greater than those obtained from DCB tests. Aspects of these measurements that lead to critical discussion are mainly based on the application of the indentation theory to thermal spray coatings since these materials are highly anisotropic. Thus, obtaining a symmetrical crack pattern during any test is never assured, since the coating microstructure has many features that influence their formation and propagation, and therefore the so-determined values are often highly variable. For example, the Weibull modulus of an alumina coating is 0.5 and the modulus of an alumina-titania coating is 0.8. The other main point, as will be discussed in the following section, is that coatings are highly anisotropic throughout their thickness and thus randomly placed indentation fracture mechanics tests would not be expected to have consistent values.

2.5.2. Anisotropy of thermally sprayed coatings. The microstructure of thermally sprayed coatings is a mix of lamellae, pores of varying geometry, and oxides, etc. It is recognized that the coating is not homogeneous and microhardness measurements can be used to examine any anisotropy. The mean values of microhardness and the distributions of data sets across the coating thickness change with respect to the test position [69]. Hence, characterizing thermally sprayed coatings by only their hardness is of limited value, since hardness depends on the precise location of the measurement. However, the microhardness measurements can quantify the material property variation in the specimen if the Weibull modulus is determined. In this fashion it was found that the variability of surface properties is greater compared to the properties throughout the specimen cross-section. The morphology of microhardness indents also changes and this feature can be used to study the variation in homogeneity and stress concentration within the specimen.

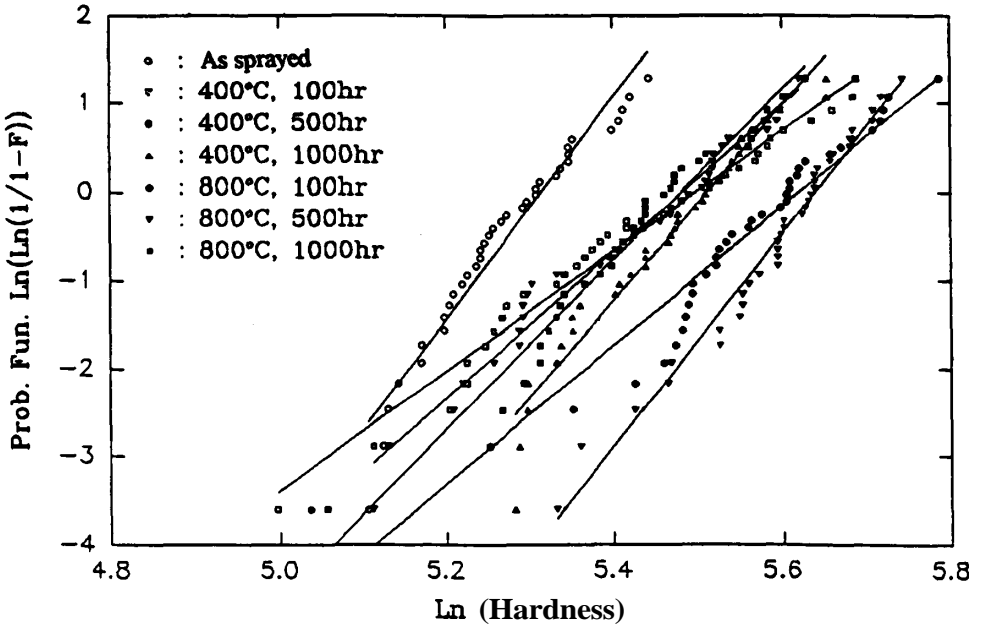


Fig. 22. Weibull plots for microhardness data for as-sprayed and aged samples within the bond coat.

As shown in Fig. 22, the Weibull modulus fluctuates and suggests that the data distributions are a reflection of microstructural changes in the bond coat. For example, the variation in ' m ' may imply the formation and distribution of oxides and crack networks.

2.5.3. Interpretation to lifetime. Microhardness measurements have been used to monitor coating behavior after thermal treatments [70]. For example, a series of thermal barrier coatings (a NiCoCrAlY intermetallic bond coat and Ce-stabilized zirconia layer) aged at different times and temperatures (at 400 and 800°C for 100, 500, and 1000 h) were tested for microhardness to assess any material property changes [71]. The major failure mechanisms of thermal barrier coatings are oxidation within the bond coat and cracking due to thermal expansion mismatch within the coating system. This can be reflected by the hardness variation and, in the future, a failure model and lifetime prediction may be based on the analysis of such data.

Temperature effects were noticed in the coating systems. For ceramic coatings, microcracks produced by thermal expansion mismatch may have different sizes and densities. These cracks will be responsible for the variation of mechanical properties. At the same time, the oxide film surrounding the lamellae within the bond coat should have different thicknesses according to the oxidation kinetics at various temperatures. These oxide films, though they may contribute to the increase of microhardness, decrease the adhesion strength of the bond coat. Schematic illustrations of mechanisms that cause coating variation are presented in Fig. 23. Non-monotonic response of hardness and the low Weibull modulus imply complex processes such as stress relaxation, growth of oxides within the bond coat, and phase change.

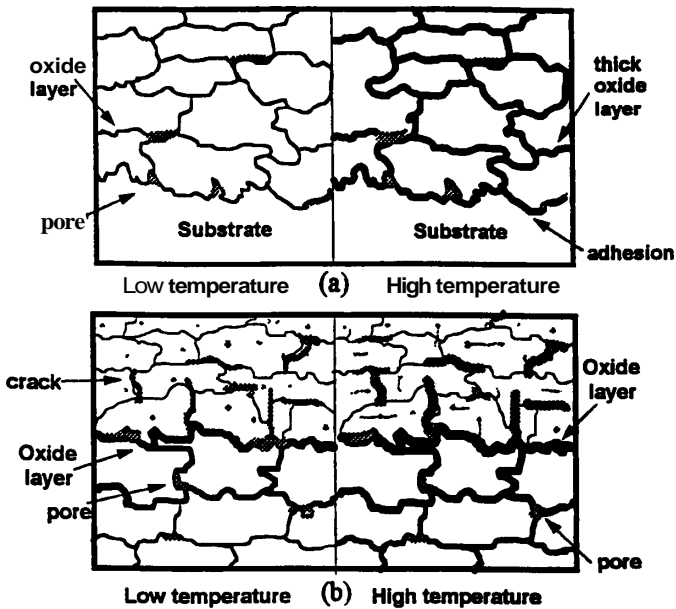


Fig. 23. Physical model of (a) the bond coat-substrate interface and (b) the bond coat-ceramic coating interface.

Thermal cycling of TBCs not only deteriorates the strength of the material at and near the bond coat interface, but also reduces the reliability of the ceramic thermal barrier layer. Microhardness measurements can be used to quantify the material property variation in the specimen. Weibull modulus values obtained in the study show that the reliability of the ceramic coating decreases from 10.5 before cycling to 5.5 after thermal cycling. The wide scatter in the hardness data indicates the variable nature of stress concentration at the test location.

Thus, increasing the reliability of coatings by controlling the variable nature of the material properties requires that the mechanical response throughout coatings be precisely quantified. Microhardness has been selected since this has been used by many authors not only to characterize specific coatings, but also to compare coatings formed from different feedstock materials, spray process, and process parameters, as well as many other properties.

2.6. Other methods

2.6.1. The scratch test. The scratch test, originally studied by Benjamin and Weaver [72], is often used to characterize thin hard coatings, such as TiN and TiC [73, 74]. In this test, a loaded Rockwell C diamond stylus is drawn across the coating surface under either constant or gradually increasing load. In one variation of the test, the AE is also monitored during the scratching procedure so that the critical load ' L_C ' for failure can be measured. The failure morphology is examined by optical microscopy or scanning electron microscopy. If interfacial, cohesive, or a mixed failure mode is observed, then L_C is used as a qualitative value of coating-substrate adhesion.

Three contributions to coating loss have been identified for the scratch

adhesion test [75–78], these being an elastic/plastic indentation (a ploughing component), and internal stress component, and a tangential frictional stress (an adhesion component).

Bull et al. [76] discussed the importance of frictional drag and suggested that under certain limitations the applied load, together with the scratched cross-sectional area, can be a convenient means of predicting the adhesion of thin coatings. Sekler et al. [77] discussed techniques to determine the critical load, and the failure modes in the scratch test were recently reviewed by Bull [78].

The scratch test has been applied in the evaluation of thermally sprayed coatings [52, 79–82]. The major problem for utilization is that all the theories were developed based on thin coatings and may no longer be appropriate for bulk coatings. Das et al. [52], in studying plasma sprayed yttria-stabilized zirconia (YSZ) coatings, proposed a method for the determination of the critical load and discussed the effect of the loading rate dL/dt and the scratch table speed dx/dt . Beltzung et al. [81, 82] performed scratch tests on the cross-section of alumina-based coatings. A half-cone-shaped fracture was formed as the indenter approached the free surface. The height of this cone can be related to the cohesive strength or intrinsic fracture toughness of the coating. Interfacial cracking may also occur and can be utilized as a measure of the adhesion strength.

2.6.2. Some tests not covered. There are many other methods that can be employed to evaluate adhesion in the qualitative or quantitative sense. The following are some examples:

- (1) wear tests [83, 84], which are related to the interfacial or cohesive strength of coatings;
- (2) thermal tests [85, 86] during thermal cycling and thermal shock protocols that influence the adhesion strength during heating and cooling processes;
- (3) shear tests [87, 88], which may best reflect the in-service conditions;
- (4) modified short bar [89] and crack-opening displacement methods [90] for fracture toughness tests.

There is still no ideal adhesion test which can satisfy all requirements. Modifications of existing techniques and designing new methods can further improve adhesion tests.

3. DEGRADATION AND FAILURE OF THERMALLY SPRAYED COATINGS

3.1. Failure mechanisms

Thermally sprayed coatings have been used widely in applications varying from biomaterials to thermal barrier coatings [91]. Coating failure can occur by one or more mechanisms such as surface damage (e.g. wear or corrosion), elastic or plastic deformation, fracture, etc. The degradation or failure of coatings is fundamentally related to the decrease of adhesion and cohesion strength, both of which cause spallation. Fundamental studies on failure mechanisms, especially for TBCs, have been discussed by NASA [92].

Thermal barrier coatings, usually comprising a metallic bond coat and a ceramic coating, endure detrimental thermal and chemical environments. General failure modes include thermal–mechanical ceramic failure, oxidation bond coat failure, hot corrosion, erosion, and fatigue [93]. The thermal variations and

inelastic strain due to interfacial oxidation, which leads to crack propagation and coating spallation, should exacerbate coating failure. Meanwhile, phase transformation and bond coat plasticity (or pseudo-elasticity) may also contribute to these mechanism(s). It has been suggested that failure is the result of slow crack growth and microcrack link-up within the ceramic which takes place in the ceramic layer close to the bond coat interface.

Chang *et al.* [94] used finite element analysis to calculate the stress field within a hypothetical wavy interface and found that radial stress would promote crack propagation. The stress owing to the thermal expansion mismatch can be estimated as [95]

$$\sigma_{x,y} = \Delta\alpha(T_{\text{cool}} - T_{\text{hot}}) \frac{E_c}{(1 - \nu_c)} \quad (5)$$

where $\Delta\alpha$ is the difference in thermal expansion coefficients between the substrate and coating, T_{cool} is the lower temperature to which a coated specimen cooled, T_{hot} is the upper temperature of a stress-free state, E_c is the elastic modulus of the ceramic, and ν_c is Poisson's ratio of the ceramic.

A representation of the thermal-mechanical properties resulting from the coating splat structure is shown in Fig. 24. It has generally been recognized that the coating failure is 'time-at-temperature' dependent, especially for oxidation. Macro- and micro-cracking will decrease the adhesion strength of the system and thus appropriate interpretation of the data obtained from adhesion measurements may be beneficial to improving the reliability and durability of the coatings.

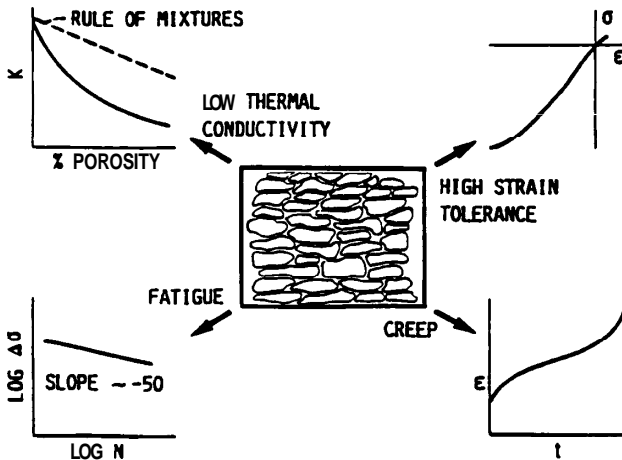


Fig. 24. Schematic representation of thermal-mechanical properties resulting from the coating splat structure of a plasma-sprayed thermal barrier coating. The diagram represents the influence of microstructure on the thermal conductivity, the stress vs. strain response, fatigue, and creep properties [93].

3.2. Lifetime modeling

A thermal barrier coating life model was proposed by Miller [95] based on the assumption that oxidation is the 'single most important factor' that limits coating lifetime. An oxidation-based model was used to calculate the cycles to failure as a

function of heating cycle duration. The coating life can be expressed by the oxidative weight gain and oxidation-induced strain as

$$\sum_{N=1}^{N_f} \left[\left(1 - \frac{\epsilon_r}{\epsilon_f} \right) \left(\frac{W_N}{W_C} \right)^m + \frac{\epsilon_r}{\epsilon_f} \right]^b = 1 \quad (6)$$

where N is the number of cycles, N_f is the number of cycles to failure, ϵ_r is the radial strain, ϵ_f is the failure strain, W_N is the oxidative weight gain at cycle N , W_C is the critical weight gain which would lead to failure in a single cycle, m is the relationship between effective strain and weight gain, and b is the subcritical crack-growth exponent.

The NASA-sponsored HOST program contributed more effort to model the TBC life [96–98]. Hillery *et al.* [96] used time-dependent, nonlinear finite element analysis to model the stress and strain within the coating system and expressed the life model as

$$\Delta \epsilon_{RZ} + 0.4 \Delta \epsilon_R = 0.121 N_f^{-0.486} \quad (7)$$

where $\Delta \epsilon_{RZ}$ is the shear strain range, $\Delta \epsilon_R$ is the normal strain range, and N_f is the number of cycles to failure.

Strangman *et al.* [97] expressed the TBC life as a function of bond coat oxidation, zirconia transformation, and damage due to molten salt deposits. The empirical equation was

$$\text{TBC life} = \frac{(t^{0.25} + 0.181) \text{MTBREF}}{\{\exp[-0.015 T + C_1]\}^{-1} + \{\exp[-0.041 T + C_2]\}^{-1}} \quad (8)$$

where MTBREF is the multi-temperature burner rig experience factor; T is the temperature (in K); t is the time; and C_1 and C_2 are constants.

DeMasi *et al.* [98] considered the fatigue performance and expressed the relationship between strain and the oxide layer thickness, δ , as

$$\Delta \epsilon_f = \Delta \epsilon_{f_0} \left(\frac{1 - \delta}{\delta_c} \right)^c + \Delta \epsilon_i \left(\frac{\delta}{\delta_c} \right)^d \quad (9)$$

where $\Delta \epsilon_f$ is the strain, $\Delta \epsilon_{f_0}$ is the oxidation strain, $\Delta \epsilon_i$ is the inelastic strain, δ is the oxide thickness at a particular cycle number, δ_c is the critical oxide thickness, and c and d are constants.

Recently, Meier *et al.* [99] studied TBC deposited by the electron beam PVD fatigue life model and gave

$$N = \left[\left(\frac{\Delta \epsilon_{ff}}{\Delta \epsilon} \right) \left(1 - \frac{\delta}{\delta_c} \right)^c + \left(\frac{\delta}{\delta_c} \right)^c \right]^b \quad (10)$$

where N is the cyclic life, $\Delta \epsilon_{ff}$ is the furnace failure strain, $\Delta \epsilon$ is the strain range, δ is the oxide thickness at a particular cycle number, δ_c is the critical oxide thickness, and b and c are constants ($b = 7.64$, $c = 1.0$).

The lifetime modeling of active in-service engineering components is a more complex problem and further effort is in progress.

4. CONCLUDING REMARKS

The measurement of the adhesion of thermally sprayed materials is, at least on the

conceptual level, a routine operation. The tensile adhesion method as detailed in ASTM C633 is simple and often used in industry for ranking different coatings. However, the major shortcoming of this test is that it does not promote any understanding of coating performance, i.e. how coatings can be designed to be more functional. Thus, the present paper has addressed other methods based on fracture mechanics and mechanism-based studies.

The design of experiments with regard to material property optimization of coatings is another area of intense effort. Experimental protocols which are based on Taguchi and response surface methodology allow engineers efficient and viable ways to optimize the process parameters [100, 101]. Such statistical methods are executed to discriminate key parameters which induce the variation of coating properties. The signal-to-noise ratios of the processing parameters are derived from such studies [102]. The Taguchi method does have some shortcomings and limitations [103] but it is a simple and powerful process control procedure.

The coating should be considered as part of the overall component system and therefore current trends are to design the coating as an integral part of the component assembly rather than as an add-on to the substrate. Whereas the property of coating adhesion to the substrate is of principal interest, there is still no single measurement which can satisfy all the requirements for determining material properties. Standardization of measurements, which may be achieved by improving existing experimental techniques or by the combination of two or more techniques, will aid future coating development. Finally, a coating design (i.e. both microstructural and mechanical engineering designs) which is based on lifetime modeling is the critical information that should be forthcoming from any test method. Such designs will increase the knowledge-base and understanding of thermal sprayed materials and coatings so that their reliability and application will grow.

Acknowledgements

We wish to thank the Alcoa Foundation for supporting parts of this work related to examining failure mechanisms of alumina. We thank Paul S. Fussell and Roger Kaufold as the managers of our program.

REFERENCES

1. T. N. Rhys Jones, *Surface Coat. Technol.* **43/44**, 402–415 (1990).
2. K. T. Scott and R. Kingswell, in: *Advanced Surface Coatings*, D. S. Rickerby and A. Matthews (Eds), pp. 217–243. Chapman and Hall, New York (1991).
3. J. H. Zatt, *Annu. Rev. Mater. Sci.* **13**, 9–42 (1983).
4. L. E. Weiss, F. B. Prinz, D. A. Adams and D. P. Siewiorek, *J. Thermal Spray Technol.* **1**, 231–237 (1992).
5. K. Neufuss, B. Kolman, J. Dubsy and P. Chraska, *Proc. AustCeram* **92**, Melbourne, 16–21 August pp. 124–129 (1992).
6. C. C. Berndt (Ed.), 1992 International Thermal Spray Conference and Exposition, 28 May–5 June, *Proceedings: Thermal Spray: International Advances in Coatings Technology*, Orlando, FL. ASM International, Materials Park, OH (1992).
7. T. F. Bernecki (Ed.), 1991 National Thermal Spray Conference and Exposition, 4–10 May, *Proceedings: Thermal Spray Coatings: Properties, Processes and Applications*, Pittsburgh, PA. ASM International, Materials Park, OH (1992).

8. S. Blum-Sandmeier, H. Eschnauer, P. Huber and A. R. Nicoll (Eds), *2nd Plasma-Technik-Symposium, Proceedings*, Plasma-Technik AG, Wohlen/Switzerland, Hafliger Druck AG, Wettingen (1991).
9. R. McPherson, *Surface Coat. Technol.* **39/40**, 173–181 (1989).
10. H. Herman, *Sci. Am.* 256, 112–117 (1989).
11. K. L. Mittal (Ed.), in: *Adhesion Measurement of Thin Films, Thick Films, and Bulk Coatings*, ASTM STP640, pp. 5–17. American Society for Testing and Materials, Philadelphia, PA (1978).
12. K. L. Mittal (Ed.), in: *Adhesion Measurement of Thin Films, Thick Films, and Bulk Coatings*, ASTM STP640, American Society for Testing and Materials, Philadelphia PA (1978).
13. R. L. Patrick (Ed.), *Treatise on Adhesion and Adhesive*, Vol. 1. Marcel Dekker, New York (1967).
14. D 907-91b, *Terminology of Adhesives*, American Society for Testing and Materials, Philadelphia, PA (1991).
15. J. Comyn, *Int. J. Adhesion Adhesives* 10, 161–165 (1990).
16. A Matting and H.-D. Steffens, *Metallwiss. Tech.* 17, 583–593, 905–922, 1213–1230 (1963). Available under Translations Register Index No. 72–14247-13H.
17. M. D. Thouless, *Mater. Res. Soc. Symp. Proc.* **119**, 51–62 (1988).
18. B. R. Lawn and T. R. Wilshaw (Eds), *Fracture of Brittle Solids*. Cambridge University Press, Cambridge (1975).
19. C. C. Berndt and R. McPherson, *Trans. Int. Eng.* **6**, 53–58 (1981).
20. C. C. Berndt, in: *Advances in Fracture Research*, Vol. 4, S. R. Valluri, D. M. R. Taplin, P. Rama Rao, J. F. Knott and R. Dubey (Eds), pp. 2545–2552. Pergamon Press, Oxford (1984).
21. G. N. Heintze and R. McPherson, *Surface Coat. Technol.* **34**, 15–23 (1988).
22. C. C. Berndt, Ph.D. Thesis, Monash University, Australia (1980).
23. P. Ostojic, Ph.D. Thesis, Monash University, Australia (1986).
24. K. L. Mittal, *J. Adhesion Sci. Technol.* 1, 247–259 (1987).
25. D. S. Rickerby, *Surface Coat. Technol.* 36, 541–557 (1988).
26. S. J. Bull and D. S. Rickerby, *Br. Ceram. Trans. J.* 88, 177–183 (1989).
27. P. R. Chalker, S. J. Bull and D. S. Rickerby, *Mater. Sci. Eng.* **A140**, 583–592 (1991).
28. B. A. Lyashenko, V. V. Rishin, V. G. Zil'berberg and S. Yu. Sharivker, *Sov. Powder Metall. Meth. Ceram.* 8, 331–334 (1969).
29. B. M. Zakharov, M. G. Trofimov, L. I. Guseva, Y. I. Golovkin, A. A. Kononov and V. V. Vinokurova, *Sov. Powder Metall. Met. Ceram.* 9, 925–929 (1970).
30. W. E. Stanton, in: *Proc. 7th Int. Metal Spraying Conf.*, 10–14 Sept. 1973. pp. 157–164, 312–314. The Welding Institute, Cambridge (1974).
31. T. Suhara, K. Kitajima and S. Fukada, in: ref. 30, pp. 179–184.
32. N. N. Rykalin, *Pure Appl. Chem.* 48, 179–194 (1976).
33. V. E. Belashchenko and Y. B. Chernyak, in: ref 6, pp. 433–437.
34. R. L. Apps, *Chem. Eng.* 292, 769–773 (1974).
35. V. Wilms and H. Herman, *Thin Solid Films* 39, 251–262 (1976).
36. T. J. Steeper, D. J. Varacalle, Jr., G. C. Wilson, W. L. Riggs (II), A. J. Rotolico and E. Nerz, in: ref. 6, pp. 415–420.
37. J. O. Outwater and D. J. Gerry, *J. Adhesion* 1, 290–298 (1969).
38. J. A. Kies and A. B. J. Clark, in: *Fracture 1969, Proceedings of the 2nd International Conference*, Brighton, P. L. Platt (Ed.), Chapman and Hall, London (1969).
39. S. J. Howard and T. W. Clyne, *Surface Coat. Technol.* 45, 333–342 (1991).
40. P. F. Becher and W. L. Newell, *J. Mater. Sci.* **12**, 90–96 (1977).
41. P. F. Becher, W. L. Newell and S. A. Halen, in: *Fracture Mechanics of Ceramics*, R. C. Bradt, D. P. H. Hasselman and F. F. Lange (Eds), Vol. III, pp. 463–471. Plenum Press, New York (1978).
42. W. D. Bascom and J. L. Bitner, *J. Mater. Sci.* 12, 1401–1410 (1977).
43. S. Mostovoy, P. B. Crosley and E. J. Ripling, *J. Mater.* 2, 661–681 (1967).
44. G. N. Heintze and R. McPherson, *Surface Coat. Technol.* 36, 125–132 (1988).
45. G. N. Heintze and R. McPherson, in: 1987 National Thermal Spray Conference and Exposition, 14–17 Sept., *Proceedings: Thermal Spray: Advances in Coatings Technology*, Orlando, FL, D. L. Houck (Ed.), pp. 271–275. ASM International Materials Park, OH (1988).
46. P. Ostojic and R. McPherson, *J. Am. Ceram. Soc.* 71, 891–899 (1988).

47. M. J. Noone and R. L. Mehan, in: *Fracture Mechanics of Ceramics*, R. C. Bradt, D. P. H. Hasselman and F. F. Lange (Eds), Vol. 1, pp. 201–229. Plenum Press, New York (1974).
48. *Acoustic Emission*, STP505, American Society for Testing and Materials, Philadelphia PA (1972).
49. J. R. Matthews (Ed.), *Acoustic Emission*, Gordon and Breach, New York (1983).
50. T. C. Nerz, J. E. Nerz, B. A. Kushner, A. J. Rotolico and W. L. Riggs, in: ref. 6, pp. 405–414.
51. L. C. Cox, *Surface Coat. Technol.* **36**, 807–815 (1988).
52. D. K. Das, M. P. Srivastava, S. V. Joshi and R. Sivakumar, *Surface Coat. Technol.* **46**, 331–345 (1991).
53. M. M. Mayuram and R. Krishnamurphy, in: ref. 6, pp. 711–715.
54. N. Iwamoto, M. Kamai and G. Ueno, in: ref. 6, pp. 259–265.
55. H. Nakahira, Y. Harada, N. Mifune, T. Yogoro and H. Yamane, in: ref. 6, pp. 519–524.
56. H. L. Dunegan, *Prevention of Structural Failure*, pp. 86–113, ASM, Materials Park, OH (1975).
57. T. Tsuru, A. Sagara and S. Haruyama, *Corrosion* **43**, 703–707 (1987).
58. F. Bordeaux, C. Moreau and R. G. Saint Jacques, *Surf: Coat. Technol.* **54/55**, 70–76 (1992).
59. C. C. Berndt, *J. Mater. Sci.* **24**, 3511–3520 (1989).
60. C. C. Berndt (Ed.), *Basic Acoustic Emission*. Gordon and Breach, New York (1991).
61. C. C. Berndt and R. A. Miller, *Thin Solid Films* **119**, 173–184 (1984).
62. C. C. Berndt, in: *Proc. Thermal Barrier Coatings Workshop*, 21–22 May, pp. 127–137. NASA Lewis Research Center, Cleveland, OH (1985).
63. B. Lawn and R. Wilshaw, *J. Mater. Sci.* **10**, 1049–1081 (1975).
64. C. Richard, J. Lu, J. F. Flavenot, G. Beranger and F. Decomps, in: ref. 6, pp. 11–16.
65. J. G. Binner and R. Stevens, *Trans. Br. Ceram. Soc.* **83**, 168–172 (1984).
66. H. Nayeab-Hashemi and C. A. Tracy, *Exp. Mech.* No. 12, 366–372 (1991).
67. G. K. Beshish, C. W. Florey, F. J. Worzala and W. J. Lenling, *J. Thermal Spray Technol.* **2**(1), 35–38 (1993).
68. R. Dal Maschio, V. M. Sgavo, L. Bertamini and E. Galvanetto, in: ref. 6, pp. 947–951.
69. C. C. Berndt, J. Karthikeyan, R. Ratanaraj and Yang Da Jun, in: ref. 7, pp. 199–203.
70. C. C. Berndt, J. Ilavsky and J. Karthikeyan, in: ref. 6, pp. 941–946.
71. C. K. Lin and C. C. Berndt, in: 1993 National Thermal Spray Conference and Exposition, 7–11 June, *Proceedings: Thermal Spray Coatings: Research, Design and Application*, Anaheim, CA. C. C. Berndt and T. F. Bernecki (Eds.), pp. 561–568. ASM International, Materials Park, OH (1993).
72. P. Benjamin and C. Weaver, *Proc. R. Soc. London, Ser. A* **254**, 163 (1960).
73. A. J. Perry, J. Valli and P. A. Steinmann, *Surface Coat. Technol.* **36**, 559–575 (1988).
74. C. Julia-Schmutz and H. E. Hintermann, *Surface Coat. Technol.* **48**, 1–6 (1991).
75. P. J. Burnett and D. S. Rickerby, *Thin Solid Films* **154**, 403–416 (1987).
76. S. J. Bull, D. S. Rickerby, A. Matthews, A. Leyland, A. R. Pace and J. Valli, *Surface Coat. Technol.* **36**, 503–517 (1988).
77. J. Sekler, P. A. Steinmann and H. E. Hintermann, *Surface Coat. Technol.* **36**, 519–529 (1988).
78. S. J. Bull, *Surface Coat. Technol.* **50**, 25–32 (1991).
79. C. W. Anderson and K. H. Heffner, in: ref. 6, pp. 695–704.
80. M. Gudge, D. S. Rickerby, R. Kingswell and K. T. Scott, in: 1990 National Thermal Spray Conference and Exposition, 20–25 May, *Proceedings: Thermal Spray Research and Application*, Long Beach, CA. T. F. Bernecki (Ed.), pp. 331–337. ASM International, Materials Park, OH (1991).
81. E. Lopez, F. Beltzung and G. Zambelli, *J. Mater. Sci. Lett.* **8**, 346–348 (1989).
82. F. Beltzung, G. Zambelli, E. Lopez and A. R. Nicoll, *Thin Solid Films* **181**, 407–415 (1989).
83. E. Lugscheider, P. Jokiel, G. Purshe, O. Roman and K. Yushchenko, in: ref. 6, pp. 647–651.
84. K. Furukubo, S. Oki and S. Gohda, in: ref. 6, pp. 705–709.
85. R. C. Hendricks and G. McDonald, *Assessment of Variations in Thermal Cycle Life Data of Thermal Barrier Coated Rods*, NASA TM-81743 (1981).
86. H.-D. Steffens and Fischer, *Surface Coat. Technol.* **32**, 327–338 (1987).
87. S. J. Grisaffe, *Analysis of Shear Bond Strength of Plasma-Sprayed Alumina Coatings on Stainless Steel*, NASA TN D3113 (1965).
88. H. Grützner and H. Weiss, *Surface Coat. Technol.* **45**, 317–323 (1991).
89. K. K. Schweitzer, M. H. Zeihl and Ch. Schwaminger, *Surface Coat. Technol.* **48**, 103–111 (1991).

90. M. J. Filaggi and R. M. Pilliar, *J. Mater. Sci.* **26**, 5383–5395 (1991).
91. R. A. Miller, *Surface Coat. Technol.* **30**, 1–11 (1987).
92. Proc. Thermal Barrier Coatings Workshop, NASA Lewis Research Center, Cleveland, OH, 21–22 May, 1985.
93. R. A. Miller, *J. Eng. Gas Turbines Power* **111**, 301–305 (1989).
94. G. C. Chang, W. Phucharoen and R. A. Miller, *Surface Coat. Technol.* **30**, 13–28 (1987).
95. R. A. Miller, *J. Am. Ceram. Soc.* **67**, 517–521 (1984).
96. R. V. Hillery, B. H. Pilsner, R. L. McKnight, T. S. Cook and M. S. Hartle, *Thermal Barrier Coating Life Prediction Model*, Final Report, NASA CR-180807 (1987).
97. T. E. Strangman, J. Neumann and A. Liu, *Thermal Barrier Coating Life Prediction Model Development*, Final Report, NASA CR-179648 (1987).
98. J. T. DeMasi, M. Ortiz and K. D. Sheffler, *Thermal Barrier Coating Life Prediction Model Development*, Phase I Final Report, NASA CR-182230 (1989).
99. S. M. Meier, D. M. Nissley and K. D. Sheffler, *Thermal Barrier Coating Life Prediction Model Development*, Phase II Final Report, NASA CR-189111 (1991).
100. G. Taguchi and S. Konishi, *Taguchi Methods, Orthogonal Arrays and Linear Groups*, American Supplier Institute, Dearborn, MI (1987).
101. P. Ross, *Taguchi Techniques for Quality Engineering*, McGraw-Hill, New York (1988).
102. G. E. P. Box, *Technometrics* **30**, 1–17 (1988)
103. S. Bisgaard, in: ref. 80, pp. 661–667.